Structural Refinement of the Tubulin Ligand (+)-Discodermolide to Attenuate Chemotherapy-Mediated Senescence

Boying Guo, Alicia Rodriguez-Gabin, Andrea E. Prota, Tobias Mühlethaler, Nan Zhang, Kenny Ye, Michel O. Steinmetz, Susan Band Horwitz, Amos B. Smith III, and Hayley M. McDaid

Department of Chemistry, Monell Chemical Senses Center and Laboratory for Research on the Structure of Matter, University of Pennsylvania, Philadelphia, Pennsylvania 19104 (B.G., N.Z., A.B.S., III); and
Departments of Molecular Pharmacology (A. R-G., S.B.H., H.M.D.), Epidemiology (K.Y.) and Medicine (H.M.D.), Albert Einstein College of Medicine, Bronx, NY 10461 and
Laboratory of Biomolecular Research, Division of Biology and Chemistry, Paul Scherrer Institut, CH-5232 Villigen, Switzerland (A.E.P., T.M., M.O.S.); and University of Basel, Biozentrum, 4056 Basel, Switzerland (M.O.S.)

Running Title: Synthesis and Evaluation of Novel (+)-Discodermolide Analogs

Corresponding Author:

Hayley McDaid, Ph.D., Albert Einstein College of Medicine, Department of Molecular Pharmacology F249b, 1300 Morris Pk Ave, Bronx NY 10461. Phone: 718-430-8829; hayley.mcdaid@einsteinmed.org

Nonstandard abbreviations: AUC, Area under the curve; CIS, Chemotherapy-induced senescence; DDM, Discodermolide; EC_{50}, potency - concentration at half-maximal effect; E_{Max}, efficacy - maximum response achievable; ROS, reactive oxygen species; SAR, Structure activity relationship; SASP, Senescence associated secretory phenotype; TNBC, Triple Negative Breast Cancer; NADPH, Nicotinamide Adenine Dinucleotide Phosphate Hydrogen; MTS, 3-(4,5-Dimethylthiazol-2-yl)-5-(3-carboxymethoxyphenyl)-2-(4-sulfophenyl)-2H-tetrazolium; H2DCFDA, 2',7'-dichlorodihydrofluorescein diacetate.

ABSTRACT

The natural product (+)-discodermolide (DDM) is a microtubule stabilizing agent and potent inducer of senescence. We refined the structure of DDM and evaluated the activity of novel congeners in triple negative breast and ovarian cancers; malignancies that typically succumb to taxane-resistance. Previous structure-activity analyses identified the lactone and diene as moieties conferring anti-cancer activity; thus identifying priorities for the structural refinement studies described herein. Congeners possessing the monodiene with a simplified lactone had superior anti-cancer efficacy relative to Taxol, particularly in resistant models. Specifically, one of these congeners, B2, demonstrated (i) improved pharmacologic properties, specifically, increased E_{Max} and AUC, and decreased EC_{50}; (ii) a uniform dose-response profile across genetically heterogeneous cancer cell lines relative to Taxol or DDM; (iii) reduced propensity for senescence induction relative to DDM; (iv) superior long-term activity in cancer cells versus Taxol or DDM, and (v) attenuation of metastatic characteristics in treated cancer cells. To contrast the binding of B2 versus DDM in tubulin, X-ray crystallography studies revealed a shift in the position of the lactone ring associated with removal of the C2-methyl and C3-hydroxyl. Thus, B2 may be more adaptable to changes in the taxane site relative to DDM that could account for its favorable properties. In conclusion, we have identified a high-efficiency DDM congener with broad range anti-cancer efficacy that also has decreased risk of inducing chemotherapy-mediated senescence.

Significance Statement

Here, we describe the anti-cancer activity of novel congeners of the tubulin-polymerizing molecule (+)-discodermolide. A lead molecule is identified that exhibits an improved dose-response profile in taxane-sensitive and -resistant cancer cell models, diminished risk of chemotherapy-mediated senescence and suppression of tumor cell invasion endpoints. X-ray crystallography studies

identify subtle changes in the pose of binding to β-tubulin that could account for the improved anti-cancer activity. These findings support continued pre-clinical development of discodermolide, particularly in the chemorefractory setting.

Introduction

(+)-Discodermolide (DDM, Fig. 1A) is a potent inducer of tubulin polymerization that has been evaluated as a chemotherapeutic in the taxane-refractory setting. However, despite its promise as anti-cancer molecule, DDM caused serious interstitial pneumopathy in clinical evaluation (Mita et al., 2004); a condition typically associated with fibrosis and senescence (Jones, 2018). We previously characterized DDM as a potent inducer of chemotherapy-induced senescence (CIS) (Chao et al., 2011; Klein et al., 2005; Nadaradjane et al., 2018), defined as prolonged exit from proliferation that is distinct from quiescence.

It is widely accepted that anticancer therapies induce senescence to varying degrees (Ewald et al., 2010). CIS has been shown to be a causative factor in bleomycin-associated pulmonary toxicity (Aoshiba et al., 2013; Schafer et al., 2017), and doxorubicin-mediated cardiac toxicity and systemic inflammation (Demaria et al., 2016). Furthermore, toxicities from cancer therapy can prevent the completion of a prescribed course of treatment, or thwart extended treatment. Aside from the collateral damage that CIS causes in non-transformed cells (Childs et al., 2015a), tumor cells can also become senescent; thereby, evading the cell-cycle dependent action of many chemotherapeutic drugs (Samaraweera et al., 2012). These cells then become a source of chronic inflammation via the Senescence Associated Secretory Phenotype (SASP), which can accelerate disease progression via multiple effects on the tumor microenvironment (Laberge et al., 2012). Finally, senescent cancer cells can resume proliferation, giving rise to more tumorigenic progeny (Chao et al., 2011; Gosselin et al., 2009; Milanovic et al., 2017). Therapy-induced aneuploidization leading to replication stress and DNA damage signaling is a known driver of CIS (Santaguida et al., 2017; Watson and Elledge, 2017). Based on our experience with DDM both in vitro and in vivo, coupled with increased awareness that CIS can mediate the toxic effects of chemotherapy, we hypothesized that DDM-mediated senescence may have contributed to its clinical toxicity.

Taxol, unlike DDM, is a comparatively weak inducer of CIS (Klein et al., 2005; Nadaradjane et al., 2018). This is hypothesized to be due to variation in the affinity and pose of binding in the Taxol-binding domain of tubulin (Prota et al., 2017), or binding of tubulin ligands to specific tubulin isotypes, or downstream effects, thereof. Prior studies of DDM structure-activity relationships (SAR) identified the lactone and diene moieties as regions for further modification that yielded congeners with superior anti-cancer activity (Simon, 2008; Smith et al., 2005; Smith and Freeze, 2007; Smith et al., 2011). For example, C(1)-C(5) simplified lactone congeners were demonstrated to have superior anti-cancer activity in cancer cell lines (Shaw et al., 2005; Smith and Xian, 2005). Coincidentally, DDM is differentially metabolized by oxidation of C(4)-C(5) of the lactone, and epoxidation of C(21)-C(22) or C(23)-C(24) diene (Fan et al., 2009). These observations led us to hypothesize that lactone and diene modifications could stabilize against oxidative metabolism and potentially influence anti-cancer activity. Building upon the original potential of DDM in the taxane-refractory setting, we set out to refine its chemical structure further.

We favored a multi-parameter analysis approach (Fallahi-Sichani et al., 2013) to analyze the activity of these novel congeners. The most commonly used metric to describe pre-clinical activity is potency, or EC_{50} (the concentration at the half-maximal effect). However, potency typically describes doses associated with proliferative arrest rather than tumor cell death. Importantly, failure to consider other features of the dose-response relationship, such as E_{Max}, (efficacy) and AUC (area under the curve - potency and efficacy in a single measure) increases the probability of selecting molecules that are strong inducers of CIS. Thus, lead DDM congeners were identified on the basis of superior pharmacologic profiles (combined use of E_{Max}, AUC and EC_{50}) relative to DDM or Taxol, coupled with propensity to induce CIS, a cell fate that is largely ignored in drug development. Collectively, our data establish novel congeners of DDM as promising therapeutics for potential use in the chemorefractory setting.

MATERIALS AND METHODS

Synthesis of Simplified DDM Congeners and X-Ray Crystallography Studies.

DDM analogs were synthesized employing the Smith gram-scale synthetic route (Smith et al., 1999; Smith et al., 2000) with minor modifications. As shown in Fig. 1B, the primary PMB ether in compounds D1-3 was selectively removed using 1.1 equivalents of BCl3 in DCM at 0 °C. The resulting primary alcohol was converted to the corresponding iodide that was used without further purification in the next step due to the instability to provide the phosphonium salt E1-3. Treatment of the phosphonium salt E1-3 with sodium bis(trimethylsilyl) amide followed by the addition of the aldehyde fragment A led to the Wittig olefination products F. The PMB protecting group was then removed using 1.2 equivalents of DDQ followed by the introduction of the carbamate. Subsequent global deprotection of the TBS groups afforded DDM analogs A1-3. DDM analogs B1-3 and C1-3 were prepared in the same manner using aldehydes B and C. All compounds were dissolved in DMSO for cell-based analysis and diluted in culture media, such that the DMSO concentration was less than 0.01%. Methods for chemical synthesis and X-Ray crystallography are provided in Supplemental Methods. Data collection and refinement statistics for T_2R-TTL-B2 are provided in Supplemental Table 6 and a simulated annealing electron density omit map highlighting the validity of the model is shown in Supplementary Fig. 5. The atomic coordinates and structure factors have been deposited in the RCSB Protein Data Bank (www.rcsb.org) under access/ion number 6SES.

Cell Lines.

Ovarian, triple negative breast (TNBC) and lung cancer cell lines (SKOV3, IGROV1, HCC38, HCC1143, BT549, HS578T, Hey, A549, NIH-H460) and the BRCA mutant TNBC cell lines HCC1937, MDA-MB-436) were purchased from ATCC and grown according to vendor recommendations. All cell lines were confirmed to be mycoplasma negative (MycoAlert detection assay, Lonza) prior to use and early passages (<20) used. BRCA mutant SUM149PT cells were

obtained from Dr. Steve Ethier, University of Michigan. All cell lines were authenticated by short tandem repeat profiling before purchase or use in this study. The resistant cell lines SKVLB and HeyTx100, derived from SKOV3 and HEY ovarian carcinoma cells, respectively, have been previously described (Bradley et al., 1989; Yang et al., 2018). Upon thawing they were grown in the presence of either vinblastine or Taxol for 2 passages, and subsequently cultured in drug-free media for a further 2 passages before use in experiments.

Cell Proliferation Assays.

Standard cell proliferation assays were performed using both sulforhodamine B (SRB) to measure total protein in adherent cells (Skehan et al., 1990). Cells were seeded at 1-3 x 10^4 cells / ml into 96-well plates, and 24h later incubated with serial dilutions of congeners (2-fold), spanning 9 dose levels, typically ranging from 250 - 1nM (n=6 wells per dose level). Cells were incubated for 3 doublings (3-7 days) without replenishing. The anti-cancer effect was computed relative to vehicle-only treated control cells and sigmoidal dose-response curves generated, as described (Fallahi-Sichani et al., 2013). Resistant cell lines required a wide range of doses (1μM - 0.01nM) to generate sigmoidal dose-response curves.

To assess the ability of congeners to suppress tumor cell proliferation long-term, duplicate plates were also set up and analyzed approximately 3 weeks later, without replenishing media or congeners. In some cases, these data were reported as drug effect without normalization as control cells continued to proliferate over the duration of the experiment and eventually died, such that normalization could not be performed. SKOV3 cells are more Taxol-sensitive relative to HEY; therefore, lower doses of all compounds were evaluated in this cell line.

For some experiments, the effect on congeners on cancer cell survival and proliferation was confirmed by MTS assay that measures NADPH / NADH production by dehydrogenase enzymes

to reduce a MTS tetrazolium compound. The advantage of this method is that viability of both adherent and non-adherent cells can be determined (Segu et al.).

Multiparameter Dose-Response Analysis.

Data were analyzed as described previously (Fallahi-Sichani et al., 2013), whereby log-transformed vlaues were fitted to a sigmoidal model using nonlinear least squares regression using the R statistical software suite (http://www.R-project.org/). The features of interest, specifically EC_{50}, E_{Max}, AUC and Hill slope were computed in R from the fitted model. AUC was estimated using numerical integration (R function integrate) over the fitted model. The code is available, upon request. E_{Max}, (efficacy) is the maximum response achievable from a molecule. EC_{50}, (potency) is the drug concentration corresponding to the half-maximal effect. AUC, (Area under the curve) is a metric that represents the area under the relative viability curve, defined as the sum of measured responses and combines potency and efficacy into one single parameter. Data were plotted in R and graphed as box and whisker plots depicting median (horizontal line) and inter-quartile range (boxes). Cancer cell lines with a Hill Slope <1 and AUC <4.0 for Taxol were categorized as Taxol–resistant (Supplemental Table S1) and analyzed as a separate cohort.

Statistics.

With the exception of multi-parameter dose-response analyses, all statistical analyses were performed using GraphPad Prism 8 (GraphPad Software Inc.). Student t tests were used to determine statistical significance of differences between the two groups. Where relevant, P values reported are from Dunnett's pot-hoc tests, adjusted for multiple variances. Equal variances analysis of E_{Max} and AUC between different congeners and Taxol was tested using a one-tailed F-test (Morgan, 1939). Differences were considered statistically significant at $P < 0.05$ (*) with 0.01-0.001 being very significant (**), 0.001-0.0001 extremely significant (***) and <0.0001 (****).

Reactive Oxygen Species Generation.

Reactive Oxygen Species (ROS) was measured in asynchronous and drug-treated HEY and A549 cells (n=6) seeded in 96-well light-sensitive plates. Cells were treated with E_{Max} doses of Taxol, DDM or congeners (A1, A2, A3, B1, B2 and B3) for 3h prior to loading with 10μM H2DCFDA (2′,7′-Dichlorodihydrofluorescein diacetate - a fluorogenic reagent that detects reactive oxygen intermediates in cells) in PBS for 40 min at 37 °C in the dark to detect intracellular ROS (Mean Fluorescence Intensity). Since congeners C had the weakest anti-cancer activity, they were not evaluated. H_2O_2 was used as a positive control. Fluorescence output was measured via plate reader (488 nm excitation / 535nm emission) and mean ROS production ± SD was determined after subtraction of background fluorescence. There was no loss of cell viability within the 3h treatment period.

Determination of Senescence.

96-well plates of cells were set up as described for cell proliferation assays to determine senescence induction. After at least 6 days treatment with various compounds (the minimal amount of time required to establish a stable senescent culture following exposure to cytotoxic compound), plates were processed for senescence associated β-galactosidase (SA-β-gal) (Itahana et al., 2007). Positive cells were identified as having blue cytoplasmic staining coupled with an enlarged, granular cytoplasm using standard light microscopy at 10-20x magnification. Data were expressed relative to the number of SA-β-gal negative cells, to differentiate between senescence and non-senescent drug-tolerant cells that survive treatment. This assay was not informative for senescent SKOV3 cells.

Transwell Invasion Assay.

Boyden Chamber assays were performed using BD Biocoat Matrigel Invasion Chambers. BT549 (metastatic TNBC) cells were seeded at 5×10^5 cells per chamber containing 0.5% serum. E_{Max}

concentrations of test compounds were added and invasion of cells through matrigel in response to a 0.5 – 10% serum gradient was quantified 20h later by fixing membranes and staining invaded cells with crystal violet. Cells were counted by microscopy, excluding edges to determine the Invasion rate (normalized to the effect of test compounds on cell viability by setting up identical plates without chamber inserts and quantifying the cell number 20h post treatment initiation). Data were expressed relative to vehicle-treated control and experiments were repeated a minimum of 3x.

Evaluation of Gene Expression in Cancer Cells Treated with Taxol or DDM Congeners.

Total RNA was isolated from cells treated with various congeners using RNAeasy, and cDNAs synthesized using the Superscript VILO Reverse Transcriptase. Real-time qRT-PCR was performed using SYBRGreen I Master (Roche) and run on a LightCycler® 480 (Roche) to determine expression of the epithelial to mesenchymal transition (EMT)-related genes, Twist, slug, snail, Vimentin and CDH2. Expression was normalized to cyclophilin B and normalized to vehicle-treated controls. Experiments were performed in triplicate. Primers were designed using primerbank (http://pga.mgh.harvard.edu/primerbank).

RESULTS

Synthesis of Simplified DDM Congeners.

The main goal of this study was to refine the chemical structure of DDM, building on prior optimization studies focused on the lactone and diene regions (Fig. 1A). We hypothesized that monosaturation of the diene and addition of a methyl at C(4) of the lactone could limit oxidation and prevent metabolic degradation (Shaw et al., 2006), potentially modulating anti-cancer activity. Additionally, since conformationally rigid 5-membered ring congeners demonstrated promising activity in previous studies (Shaw et al., 2005), diene-saturated variants of these were also synthesized (Fig. 1B), culminating in a series of congeners available for testing (Fig. 1C).

Multi-Parameter Analysis of Dose-Response Relationships Identifies Lead DDM Congeners.

The anti-cancer activity of DDM congeners was determined in a panel of genetically heterogeneous human breast (TNBC) and ovarian cancer cell lines by multi-parametric dose-response analyses, as described (Fallahi-Sichani et al., 2013). Median E_{Max}, AUC and EC_{50} values were computed for all cell lines (Supplemental Table 1) and distribution plotted (Fig. 2A). AUC and EC_{50} were statistically significantly different for DDM and Taxol across all cell lines. Moreover, congeners A2 and B2 had the most significantly increased AUC ($P<0.0001$) and EC_{50} ($P=0.0002$ - 0.0001) relative to DDM (Supplemental Table 2). No significant differences in E_{Max} were evident for any of congener versus either Taxol or DDM.

Dose-response plots for all data illustrate the variation in dose-response relationships for the four molecules, despite shared mechanism of action (Fig. 2B). DDM generated more linear shaped plots relative to the sigmoidal plots typical of Taxol and congeners B2 and A2. Variances in the median AUC or E_{Max} of the congeners relative to Taxol were evaluated using an F-test (Supplemental Table 3). The variation in median E_{Max} for B2 (but not A2) indicate some difference compared to Taxol (F statistic, $P= 0.032$), with a trend toward significance for AUC also ($P=0.070$), suggesting that B2 may generate a uniform pharmacologic response relative to Taxol. However, this statistical significance may not hold after adjusting for multiple testing.

Definition of the Optimal C(21)-C(24) Terminus and Lactone Structural Elements of DDM.

Epoxidation of the C(21)-C(22) or C(23)-C(24) diene was hypothesized to contribute to enzymatic degradation (Fan et al., 2009); therefore diene – monoene – saturated congeners were synthesized for evaluation. Saturated analogs (A3, B3 and C3) had weak anti-cancer activity irrespective of lactone, evident as high EC_{50}, and low E_{Max} and AUC (Fig. 2B, Supplemental Table 1). Median E_{Max} for diene versus monoene congeners was comparable; however monoenes (A2

and B2) had higher AUC and lower EC_{50} compared to dienes (A1 and B1) across all cell lines, though not statistically signifcant. Turning to the lactone, the addition of a second methyl group at the C(4) position to form a gem di-methyl (congeners A1-A3) was designed to block oxidative metabolism of the C(4)-C(5) bond; however, there was only a subtle difference in dose-response parameters of these analogs relative to the B series that have one methyl at C(4) (Fig. 2B). In contrast, lactone congeners with 5 membered rings (series C) had weaker anti-cancer activity relative to both the A and B series. Within C series, the diene-containing analogue, C1 was most active (Fig. 2A). Therefore, a DDM congener with a monoene and one C4-methyl is the optimal conformation for anti-cancer activity.

DDM Congeners Do Not Exhibit Significant Changes in Reactive Oxygen Species Generation.

Since DDM can be differentially oxidized at numerous sites including C(4)-C(5) and C(21)-C(22) or C(23)-C(24), we hypothesized that enzymatic hindrance at these sites could limit metabolic degradation. High reactive oxygen species (ROS) from mitochondrial oxidative damage in cells is associated with either senescence (Ziegler et al., 2015), cell death or proliferation, depending on the cellular context (Ogrunc et al., 2014; Olsen et al., 2013). We hypothesized that metabolic degradation of DDM could generate high (ROS), potentially causing senescence, therefore, we measured ROS generation as a surrogate for metabolic degradation. All congeners had reduced ROS relative to DDM within the parameters tested (Table 1 and Supplemental Fig. 1). Levels were similar across A and B series suggesting that a simplifed lactone stucture and not the C4 constituent (methyl or gem-di-methyl) had the strongest influence on ROS generation. Similiarily, there was no statistically significant difference in ROS levels that correlated with diene saturation. Taxol generated ROS at levels comparable to the positive control, H_2O_2, and at statistically higher levels compared to DDM ($P<0.05$); however, Taxol is a weak inducer of senescence (Klein et al., 2005). Furthermore, comparing ROS generation with dose-response parameters (Fig. 2) and CIS

(Fig. 4E), we conclude that ROS levels do not correlate with anti-cancer efficacy, or CIS under the conditions evaluated here.

Identification of DDM Congeners with Activity in Taxol-Resistant Cell Models.

To facilitate a nuanced dose-response relationship analysis, we dichotomized data into Taxol-resistant versus -sensitive cohorts. Resistant cell lines were identified as having AUC<4 and Hill slope <1 (Supplemental Table S4), consistent with previously described features (Fallahi-Sichani et al., 2013; Sampah et al., 2011). Analysis of sensitive cell lines indicated similar median AUC and EC_{50} among congeners A2 and B2 versus Taxol (Fig. 3). In contrast, Taxol had a weak anti-cancer effect in resistant cell lines, whereas both A2 and B2 had statistically significantly improved AUC (P=0.017) and (P=0.0072), respectively (Supplemental Table S4). Similarly, A2 and B2 had significantly improved EC_{50}.

Congener B2 has Superior Long-Term Efficacy Compared to Taxol.

Reported values for EC_{50} and E_{Max} for a given cell line often vary widely due to differences in assay type and failure to tailor assays to account for differences in doubling time (Hafner et al., 2016), though our experimental design accounted for this. Colony-forming assays can be used to monitor longer-term anti-cancer efficacy; however, low seeding densities can artificially inflate efficacy metrics (Hafner et al., 2016). To circumvent this, we extended the duration of standard proliferation assays from 3 cell doublings to approximately 3 weeks without congener replenishment, to evaluate long-term anti-cancer effect.

As shown for the ovarian cancer cell line HEY, dose-response curves for Taxol and B2 were overlapping after 3 cell doublings (Fig. 4A) indicating almost identical effect. However, by day 21 (Fig. 4B), the dose-response curve for Taxol was more shallow with substantially reduced AUC, due to re-growth of transiently growth-arrested cells. Impressively, B2 -treated cells sustained a strong anti-cancer response evident by day 21. Images of SRB-stained plates are shown at day

3 and 21 (Fig. 4C and D). Measurement of mitochondrial oxidoreductase activity in both adherent and non-adherent drug-treated cells (MTS) also confirmed these findings (Supplemental Fig. S2). Since multi-parameter analysis also indicated promising activity of congener A2, we contrasted the long-term effect of A2 versus B2 (Supplemental Fig. S2C and D) and found that both had superior long-term activity compared to Taxol; however B2 had the most sustained effect. As a control, the long-term activity of cisplatin (FDA-approved therapy for serous ovarian cancer) was determined and found to have weak anti-cancer effect in HEY cells (Supplemental Fig. S2E). In conclusion, congener B2 displayed superior short and long-term activity relative to Taxol, cisplatin and other DDM congeners. The effect of B2 was also evaluated in SKOV3 ovarian cancer cells (Supplemental Fig. S3), where short- and long-term analysis (4 days and 3 weeks) again indicated superior activity of B2 compared to Taxol.

Attenuation of CIS by Congener B2.

Since CIS is a major outcome of DDM exposure (Chao et al., 2011; Klein et al., 2005), we evaluated the lead congener, B2 for senescence inducing properties. HEY cells are amenable to senescence quantitation using the SA-β-gal assay (Itahana et al., 2007); therefore, four dose levels, approximating to $E_{Max,}$ EC_{50} and $>EC_{50}$ were evaluated for SA-β-gal positivity (Supplemental Table 5). As shown in Fig. 4E, DDM strongly induced senescence at 50nM, a dose that approximated the 6-day EC_{50}. In contrast, Taxol was a weak inducer of senescence, consistent with previous reports (Klein et al., 2005). Congener B2 had significantly reduced senescence relative to DDM at 50nM ($P<0.01$: ANOVA with post-hoc test), although the phenotype was still detected at a lower dose (Supplemental Table 5). Thus, at doses approximating the EC_{50}, congener B2 had attenuated risk of CIS relative to DDM.

We recently demonstrated that Taxol does not possess significant senolytic activity, defined as the ability to induce senescent cell death (Samaraweera et al., 2017). Cisplatin (CDDP) and the

histone deacetylase inhibitor panobinostat, however, have strong senolytic activity. Thus, we evaluated the ability of DDM and congeners B2 and A2 to kill senescent HEY or A549 cells and found that like Taxol, they possess little to no senolytic activity (Supplemental Fig. 4).

Superior Anti-Metastatic Properties of Congener B2.

Since cancer mortality is primarily due to metastatic dissemination, we investigated the effect of congener B2, Taxol and DDM on metastatic parameters in BT549 (Fig. 5), an invasive, mesenchymal TNBC cell line (Lehmann et al., 2011) images of congener-treated cells are shown to illustrate differential effects on morphology and proportion of surviving cells. The effect of the various tubulin ligands on EMT-associated genes in surviving, adherent cells was also evaluated. Expression of the transcription factors snail and slug, known regulators of EMT (Batlle et al., 2000; Nieto et al., 1994) was increased by Taxol and DDM treatment, while B2-treated cells exhibited a statistically significantly decreased expression of all 5 genes comprising the EMT signature, relative to vehicle-only control ($P>0.0001$: Unpaired t-test). The effect of Taxol, DDM or B2 on BT549 invasion through matrigel was also evaluated (Fig. 5C). All three suppressed invasion relative to vehicle-only controls; however the effect was most pronounced for DDM and B2, though not statistically significant. Thus, congener B2 treatment imparts favorable anti-metastatic properties in this aggressive model of mesenchymal TNBC.

Congener B2 Binds to the Taxane-site with a Shifted Lactone Compared to DDM.

The binding mode of DDM in the taxane pocket of β-tubulin has recently been described in great detail by X-ray crystallography (Prota et al., 2017). To provide critical insights into the molecular mechanism of action of the lead congener, B2, we determined the crystal structure of a tubulin-B2 complex to 2.0 Å resolution (Fig. 6). B2 bound to the taxane-site on β-tubulin in a very similar

hairpin conformation as DDM (Fig. 6A) and the majority of the interactions were conserved. However, compared to DDM, the absence of both the C2-methyl and the C3-hydroxyl in B2 gave rise to a loss of one hydrogen bond to the backbone of Arg369, and a re-orientation of the lactone ring in the pocket (Fig. 6B). Moreover, a smaller re-orientation of the the C23 and C24 section of the monoene sidechain was observed, which caused a minor shift of the Arg278 sidechain. These observations demonstrate that B2 binds to the taxane-site on β-tubulin. They further suggest a better adaptation capability to changes in the taxane-binding site of congener B2 compared to DDM.

We further superimposed the taxol bound MT-structure (Fig 6C, PDB ID 5SYF) onto the taxane site of the tubulin-B2 complex (rmsd of 0.99 Å over [49 C_α-atoms]). Compared to Taxol, B2 and DDM occupied the structural cavities previously reported (Prota et al., 2017) by positioning their lactone rings between the C4-acetyl and the 3'-phenyl moieties, relative to Taxol. There were also significant differences in the orientation of Arg 278 by DDM and B2 versus Taxol, which are potentially significant for future molecular dynamic studies, since amino acids Ser 277 and Arg 278 are variant among human tubulin isotypes. Overall, these data provide structual insights in support of a favorable occupation of B2 in the binding pocket of tubulin that associate with improved biological activity relative to DDM.

DISCUSSION

Cytotoxic chemotherapies cause an array of fates in tumors including apoptosis, necrosis, mitotic catastrophe and the dormancy phenotypes, quiescence and senescence. CIS is an unintended consequence of cancer treatment that imparts long-term consequences that may contribute to accelerated aging in cancer survivors and increased risk of developing a secondary malignancy, reviewed in (Childs et al., 2015b). Thus, minimizing risk of CIS is an important but underappreciated consideration in contemporary anti-cancer drug development. We have

implemented a robust strategy to select molecules that maximize tumor cell death while minimizing CIS based on increasing E_{Max} and AUC, and steepening the Hill slope (Fallahi-Sichani et al., 2013; Nadaradjane et al., 2018). This multi-parametric approach best maximizes leads for further development, evolving contemporary drug discovery beyond an EC_{50}-centric approach; thereby, lessening the risk of developing compounds that strongly induce CIS.

Although the tumor suppressive effects of senescence prevents the replication of damaged cells that could potentially become malignant; this applies primarily to young cells and tissues (Baker et al., 2011; Braumuller et al., 2013; Flach et al., 2014; Katsimpardi et al., 2014; Storer et al., 2013). However, in cancer cells the integrity of the cell cycle regulatory apparatus is compromised, such that they can escape or by-pass senescence, enabling malignant cell expansion (Damsky et al., 2015; Le Duff et al., 2018; Sharpless and Sherr, 2015). For this reason, pro-senescent cancer therapies have largely fallen out of favor due to concerns regarding chronic SASP signaling and tumor evolution (Milanovic et al., 2017). A significant exception to this, however, is the approval of combined CDK4/6 inhibitors with antiestrogens for the treatment of ER+, HER2- breast cancer. (Wolff, 2016) The mechanism of action is partially attributable to senescence induction in tumors that retain retinoblastoma function, with subsequent immune-mediated clearance in some patients (Knudsen and Witkiewicz, 2017) Thus, it is hypothesized that therapy-mediated senescence in tumors with intact G1/S checkpoint function and a low prevalence of genetic alterations can lead to favorable clinical outcome (Knudsen and Witkiewicz, 2017). However, the majority of solid malignancies approved for treatment with Taxol, including breast and ovarian cancers, do not meet these criteria; therefore, drug effect is highly variable, as demonstrated by our dose-response modeling. In light of these considerations, it is significant that the lead DDM congener, B2, has a more uniform dose-response profile relative to Taxol and DDM, despite the significant genetic variability of the cell lines tested.

We set out to define, synthesize and test congeners for potent anti-cancer activity including diminished risk of CIS, a dominant mechanism of action of DDM (Klein et al., 2005). DDM-mediated senescence is durable, based on the time it takes for resistant clones to emerge (Chao et al., 2011); therefore, it is not surprising that congener B2 also induces senescence, albeit at significantly reduced levels relative to the parent molecule. Despite justifiable concerns about inducing senescence in solid tumors, retention of some CIS activity across a narrow dose-range could impart favorable outcome, specifically in terms of longevity of the response, as demonstrated by the sustained effect of B2 after 3 weeks that was superior to Taxol. Furthermore trepidation related to sustained SASP signaling from persistent senescent cells could be allayed by our finding that cisplatin, typically administered sequentially after Taxol, is a potent senolytic that can kill senescent cancer cells (Samaraweera et al., 2017).

We are interested in uncovering mechanistic insight at the level of the tubulin-ligand interaction to account for the improved dose-response relationship of B2 relative to DDM, or Taxol. Clearly, modulation of the lactone and diene confer increased E_{Max} and AUC such that cell kill is a more prevalent mechanism of action for congeners A2 and B2. However, this may be due to mechanisms distal to tubulin polymerization, including enhanced cellular uptake and resistance to efflux and / or resistance to metabolic degradation. These attributes will be determined in future mouse studies to evaluate systemic toxicity and in vivo efficacy of these molecules.

Other explanations include mechanisms proximal to the tubulin-ligand interaction, including different binding affinity of B2 compared to DDM or Taxol; thereby, inducing differential effects on tubulin dimers and / or the microtubule lattice. To address this, we generated a crystal structure of the tubulin-B2 complex to uncover the molecular interaction and demonstrated a shift in the occupation of the lactone of B2 versus DDM in the taxane-site. Minor changes were observed at the monoene moiety. Thus, removal of both the C2-methyl and C3-hydroxyl could render B2 more

adaptable to changes in the taxane site and provide a molecular basis to account, at least partially, for the improved anti-cancer activity of B2 versus DDM.

Although the crystallography studies were done using bovine brain tubulin, we are cognizant of the fact that the tubulin family is composed of multiple isotypes, each assumed to possess functional specificity within a given cell type. It is plausible that DDM binds a specific tubulin isotype with a specialized function in G1/S checkpoint integrity or similar; such that perturbation causes potent senescence. Lactone and diene modifications could also influence binding to distinct tubulin isotypes that ultimately modulates cellular fate i.e. death versus senescence. While the lactone binding domain of human tubulins is largely invariant, there are isotype-defining amino acid changes in the diene-interacting domain that could potentially modulate tubulin-ligand interactions. Delineating such interactions would prove invaluable in guiding future structural refinements of DDM. This requires biochemical testing that presently is challenging for studies of human tubulin, although, additional studies are ongoing to address these questions and to provide critical insight into the molecular mechanism of action of B2, a promising anti-cancer molecule.

Acknowledgments

The authors acknowledge the assistance of Dr. Chia-Ping H. Yang in preparing congener stock solutions.

Authors' Contributions

Participated in research design: SBH, ABS, BG, AEP, MOS and HMD

Conducted experiments: BG and NK (chemical synthesis), ARG (cell-based analysis), TM (protein expression, purification and crystallization) and AEP (X-ray crystallography)

Contributed reagents and analytic tools: ABS and KY

Performed data analysis: ARG and HMD (cell-based analysis), KY (biostatistics) and AEP and MOS (structure analysis)

Wrote or contributed to the writing of the manuscript: HMD wrote the manuscript. BG, ARG, AEP and HMD prepared Figures and Tables. All authors discussed results and edited the manuscript.

REFERENCES

Aoshiba K, Tsuji T, Kameyama S, Itoh M, Semba S, Yamaguchi K and Nakamura H (2013) Senescence-associated secretory phenotype in a mouse model of bleomycin-induced lung injury. Experimental and Toxicologic Pathology 65(7): 1053-1062.

Baker DJ, Wijshake T, Tchkonia T, LeBrasseur NK, Childs BG, van de Sluis B, Kirkland JL and van Deursen JM (2011) Clearance of p16Ink4a-positive senescent cells delays ageing-associated disorders. Nature 479(7372): 232-236.

Batlle E, Sancho E, Francí C, Domínguez D, Monfar M, Baulida J and García de Herreros A (2000) The transcription factor Snail is a repressor of E-cadherin gene expression in epithelial tumour cells. Nature Cell Biology 2(2): 84-89.

Bradley G, Naik M and Ling V (1989) P-Glycoprotein Expression in Multidrug-resistant Human Ovarian Carcinoma Cell Lines. Cancer Research 49(10): 2790.

Braumuller H, Wieder T, Brenner E, Assmann S, Hahn M, Alkhaled M, Schilbach K, Essmann F, Kneilling M, Griessinger C, Ranta F, Ullrich S, Mocikat R, Braungart K, Mehra T, Fehrenbacher B, Berdel J, Niessner H, Meier F, van den Broek M, Haring HU, Handgretinger R, Quintanilla-Martinez L, Fend F, Pesic M, Bauer J, Zender L, Schaller M, Schulze-Osthoff K and Rocken M (2013) T-helper-1-cell cytokines drive cancer into senescence. Nature 494(7437): 361-365.

Chao SK, Lin J, Brouwer-Visser J, Smith AB, 3rd, Horwitz SB and McDaid HM (2011) Resistance to discodermolide, a microtubule-stabilizing agent and senescence inducer, is 4E-BP1-dependent. Proc Natl Acad Sci U S A 108(1): 391-396.

Childs BG, Durik M, Baker DJ and van Deursen JM (2015a) Cellular senescence in aging and age-related disease: from mechanisms to therapy. Nat Med 21(12): 1424-1435.

Childs BG, Durik M, Baker DJ and van Deursen JM (2015b) Cellular senescence in aging and age-related disease: from mechanisms to therapy. Nature medicine 21(12): 1424-1435.

Damsky W, Micevic G, Meeth K, Muthusamy V, Curley David P, Santhanakrishnan M, Erdelyi I, Platt James T, Huang L, Theodosakis N, Zaidi MR, Tighe S, Davies Michael A, Dankort D, McMahon M, Merlino G, Bardeesy N and Bosenberg M (2015) mTORC1 Activation Blocks BrafV600E-Induced Growth Arrest but Is Insufficient for Melanoma Formation. Cancer Cell 27(1): 41-56.

Demaria M, Leary MN, Chang J, Shao L, Liu S, Alimirah F, Koenig K, Le C, Mitin N, Deal AM, Alston S, Academia EC, Kilmarx S, Valdovinos A, Wang B, de Bruin A, Kennedy BK, Melov S, Zhou D, Sharpless NE, Muss H and Campisi J (2017) Cellular Senescence Promotes Adverse Effects of Chemotherapy and Cancer Relapse. Cancer Discovery 7(2):165-176.

Ewald JA, Desotelle JA, Wilding G and Jarrard DF (2010) Therapy-induced senescence in cancer. Journal of the National Cancer Institute 102(20): 1536-1546.

Fallahi-Sichani M, Honarnejad S, Heiser LM, Gray JW and Sorger PK (2013) Metrics other than potency reveal systematic variation in responses to cancer drugs. Nature chemical biology 9(11): 708-714.

Fan Y, Schreiber EM and Day BW (2009) Human liver microsomal metabolism of (+)-discodermolide. J Nat Prod 72(10): 1748-1754.

Flach J, Bakker ST, Mohrin M, Conroy PC, Pietras EM, Reynaud D, Alvarez S, Diolaiti ME, Ugarte F, Forsberg EC, Le Beau MM, Stohr BA, Mendez J, Morrison CG and Passegue E (2014) Replication stress is a potent driver of functional decline in ageing haematopoietic stem cells. Nature 512(7513): 198-202.

Gosselin K, Martien S, Pourtier A, Vercamer C, Ostoich P, Morat L, Sabatier L, Duprez L, Kint de Roodenbeke C, Gilson E, Malaquin N, Wernert N, Slijepcevic P, Ashtari M, Chelli F, Deruy E, Vandenbunder B, De Launoit Y and Abbadie C (2009) Senescence-Associated Oxidative DNA Damage Promotes the Generation of Neoplastic Cells. Cancer Research 69(20): 7917.

Hafner M, Niepel M, Chung M and Sorger PK (2016) Growth rate inhibition metrics correct for confounders in measuring sensitivity to cancer drugs. Nat Meth 13(6): 521-527.

Itahana K, Campisi J and Dimri GP (2007) Methods to detect biomarkers of cellular senescence: the senescence-associated beta-galactosidase assay. Methods Mol Biol 371: 21-31.

Jones KD (2018) Unclassifiable interstitial lung disease: a pathologist's perspective. European Respiratory Review 27(147): 170132.

Katsimpardi L, Litterman NK, Schein PA, Miller CM, Loffredo FS, Wojtkiewicz GR, Chen JW, Lee RT, Wagers AJ and Rubin LL (2014) Vascular and neurogenic rejuvenation of the aging mouse brain by young systemic factors. Science 344(6184): 630-634.

Klein LE, Freeze BS, Smith AB, 3rd and Horwitz SB (2005) The microtubule stabilizing agent discodermolide is a potent inducer of accelerated cell senescence. Cell Cycle 4(3): 501-507.

Knudsen ES and Witkiewicz AK (2017) The Strange Case of CDK4/6 Inhibitors: Mechanisms, Resistance, and Combination Strategies. Trends in cancer 3(1): 39-55.

Laberge R-M, Awad P, Campisi J and Desprez P-Y (2012) Epithelial-Mesenchymal Transition Induced by Senescent Fibroblasts. Cancer Microenvironment 5(1): 39-44.

Le Duff M, Gouju J, Jonchère B, Guillon J, Toutain B, Boissard A, Henry C, Guette C, Lelièvre E and Coqueret O (2018) Regulation of senescence escape by the cdk4–EZH2–AP2M1 pathway in response to chemotherapy. Cell Death & Disease 9(2): 199.

Lehmann BD, Bauer JA, Chen X, Sanders ME, Chakravarthy AB, Shyr Y and Pietenpol JA (2011) Identification of human triple-negative breast cancer subtypes and preclinical models for selection of targeted therapies. J Clin Invest 121(7): 2750-2767.

Milanovic M, Fan DNY, Belenki D, Däbritz JHM, Zhao Z, Yu Y, Dörr JR, Dimitrova L, Lenze D, Monteiro Barbosa IA, Mendoza-Parra MA, Kanashova T, Metzner M, Pardon K, Reimann M, Trumpp A, Dörken B, Zuber J, Gronemeyer H, Hummel M, Dittmar G, Lee S and

Schmitt CA (2017) Senescence-associated reprogramming promotes cancer stemness. Nature 553: 96.

Mita A, Lockhart AC, Chen TL, Chen K, Bochinski J, Curtright W, Cooper L, Hammond M, Rothenberg E, S. R and Sharma S (2004) A phase I pharmacokinetic (PK) trial of XAA296A (Discodermolide) administered every 3 3ks to adult patients with advanced solid malignancies. . Journal of Clinical Oncology (Meeting Abstracts) 22 (no. 14_suppl 2025).

Morgan WA (1939) TEST FOR THE SIGNIFICANCE OF THE DIFFERENCE BETWEEN THE TWO VARIANCES IN A SAMPLE FROM A NORMAL BIVARIATE POPULATION. Biometrika 31(1-2): 13-19.

Nadaradjane C, Yang CH, Rodriguez-Gabin A, Ye K, Sugasawa K, Atasoylu O, Smith AB, 3rd, Horwitz SB and McDaid HM (2018) Improved Dose-Response Relationship of (+)-Discodermolide-Taxol Hybrid Congeners. J Nat Prod 81(3): 607-615.

Nieto MA, Sargent MG, Wilkinson DG and Cooke J (1994) Control of cell behavior during vertebrate development by Slug, a zinc finger gene. Science 264(5160): 835.

Ogrunc M, Di Micco R, Liontos M, Bombardelli L, Mione M, Fumagalli M, Gorgoulis VG and d'Adda di Fagagna F (2014) Oncogene-induced reactive oxygen species fuel hyperproliferation and DNA damage response activation. Cell Death And Differentiation 21: 998.

Olsen LF, Issinger O-G and Guerra B (2013) The Yin and Yang of redox regulation. Redox Report 18(6): 245-252.

Prota AE, Bargsten K, Redondo-Horcajo M, Smith AB, 3rd, Yang CH, McDaid HM, Paterson I, Horwitz SB, Fernando Diaz J and Steinmetz MO (2017) Structural Basis of Microtubule Stabilization by Discodermolide. Chembiochem 18(10): 905-909.

Samaraweera L, Adomako A, Rodriguez-Gabin A and McDaid HM (2017) A Novel Indication for Panobinostat as a Senolytic Drug in NSCLC and HNSCC. Scientific Reports 7(1): 1900.

Samaraweera L, Liu L, Suzuki M, Horwitz SB and McDaid HM (2012) Senescence reversion contributes to acquired drug resistance. Cancer Research 72(8): Supplement 1: 4230.

Sampah MES, Shen L, Jilek BL and Siliciano RF (2011) Dose–response curve slope is a missing dimension in the analysis of HIV-1 drug resistance. Proceedings of the National Academy of Sciences 108(18): 7613-7618.

Santaguida S, Richardson A, Iyer DR, M'Saad O, Zasadil L, Knouse KA, Wong YL, Rhind N, Desai A and Amon A (2017) Chromosome Mis-segregation Generates Cell-Cycle-Arrested Cells with Complex Karyotypes that Are Eliminated by the Immune System. Developmental Cell 41(6): 638-651.e635.

Schafer MJ, White TA, Iijima K, Haak AJ, Ligresti G, Atkinson EJ, Oberg AL, Birch J, Salmonowicz H, Zhu Y, Mazula DL, Brooks RW, Fuhrmann-Stroissnigg H, Pirtskhalava T, Prakash YS, Tchkonia T, Robbins PD, Aubry MC, Passos JF, Kirkland JL, Tschumperlin DJ, Kita H and LeBrasseur NK (2017) Cellular senescence mediates fibrotic pulmonary disease. Nature Communications 8: 14532.

Segu VBG, Li G and Metz SA Use of a soluble tetrazolium compound to assay metabolic activation of intact β cells. Metabolism - Clinical and Experimental 47(7): 824-830.

Sharpless NE and Sherr CJ (2015) Forging a signature of in vivo senescence. Nature Reviews Cancer 15: 397.

Shaw SJ, Sundermann KF, Burlingame MA, Myles DC, Freeze BS, Xian M, Brouard I and Smith AB, 3rd (2005) Toward understanding how the lactone moiety of discodermolide affects activity. J Am Chem Soc 127(18): 6532-6533.

Shaw SJ, Sundermann KF, Burlingame MA, Zhang D, Petryka J and Myles DC (2006) A series of 23,24-dihydrodiscodermolide analogues with simplified lactone regions. Bioorganic & Medicinal Chemistry Letters 16(7): 1961-1964.

Simon JS (2008) The Structure Activity Relationship of Discodermolide Analogues. Mini-Reviews in Medicinal Chemistry 8(3): 276-284.

Skehan P, Storeng R, Scudiero D, Monks A, McMahon J, Vistica D, Warren JT, Bokesch H, Kenney S and Boyd MR (1990) New colorimetric cytotoxicity assay for anticancer-drug screening. J Natl Cancer Inst 82(13): 1107-1112.

Smith AB, 3rd, Kaufman MD, Beauchamp TJ, LaMarche MJ and Arimoto H (1999) Gram-scale synthesis of (+)-discodermolide. Org Lett 1(11): 1823-1826.

Smith AB, 3rd, Rucker PV, Brouard I, Freeze BS, Xia S and Horwitz SB (2005) Design, synthesis, and biological evaluation of potent discodermolide fluorescent and photoaffinity molecular probes. Org Lett 7(23): 5199-5202.

Smith AB, 3rd and Xian M (2005) Design, synthesis, and biological evaluation of simplified analogues of (+)-discodermolide. Additional insights on the importance of the diene, the C7 hydroxyl, and the lactone. Org Lett 7(23): 5229-5232.

Smith AB, Beauchamp TJ, LaMarche MJ, Kaufman MD, Qiu Y, Arimoto H, Jones DR and Kobayashi K (2000) Evolution of a Gram-Scale Synthesis of (+)-Discodermolide. Journal of the American Chemical Society 122(36): 8654-8664.

Smith AB and Freeze BS (2007) (+)-Discodermolide: Total Synthesis, Construction of Novel Analogues, and Biological Evaluation. Tetrahedron 64(2): 261-298.

Smith AB, Sugasawa K, Atasoylu O, Yang CP and Horwitz SB (2011) Design and synthesis of (+)-discodermolide-paclitaxel hybrids leading to enhanced biological activity. J Med Chem 54(18): 6319-6327.

Storer M, Mas A, Robert-Moreno A, Pecoraro M, Ortells MC, Di Giacomo V, Yosef R, Pilpel N, Krizhanovsky V, Sharpe J and Keyes WM (2013) Senescence is a developmental mechanism that contributes to embryonic growth and patterning. Cell 155(5): 1119-1130.

Watson EV and Elledge SJ (2017) Aneuploidy Police Detect Chromosomal Imbalance Triggering Immune Crackdown! Trends in Genetics 33(10): 662-664.

Wolff AC (2016) CDK4 and CDK6 Inhibition in Breast Cancer — A New Standard. New England Journal of Medicine 375(20): 1993-1994.

Yang C-PH, Wang C, Ojima I and Horwitz SB (2018) Taxol Analogues Exhibit Differential Effects on Photoaffinity Labeling of β-Tubulin and the Multidrug Resistance Associated P-Glycoprotein. Journal of Natural Products 81(3): 600-606.

Ziegler DV, Wiley CD and Velarde MC (2015) Mitochondrial effectors of cellular senescence: beyond the free radical theory of aging. Aging Cell 14(1): 1-7.

Footnotes

This work was supported by National Cancer Institute Grants [CA077263], the Breast Cancer Research Foundation, the National Foundation for Cancer Research and the Swiss National Science Foundation Grant [31003A_166608] (MOS). Research reported in this publication was also supported by the Albert Einstein Cancer Center Support Grant of the National Institutes of Health under award number [P30CA013330]. The content is solely the responsibility of the authors and does not necessarily represent the official views of the National Institutes of Health.

Fig. 1. Structure of (+)-DDM-modified congeners.
(A) Chemical structure of (+)-Discodermolide (DDM) illustrating the lactone and diene moieties.
(B) Representative synthesis of DDM analogs.
(C) Structures of the congener series (A1 - C3) available for biological analysis.

Fig. 2. Analysis of dose-response parameters for DDM, Taxol and novel DDM congeners across 12 TNBC and ovarian cancer cell lines identifies A2 and B2 as promising anti-cancer leads.
(A) Variation in dose-response parameters for DDM, Taxol (Tx) and congeners (A1 – C3) across 12 TNBC and ovarian cancer cell lines. Values were computed from sigmoidal dose-response curves. Analysis parameters are EC_{50} (potency), E_{Max} (efficacy) and AUC (potency and efficacy combined). Data are represented as box and whisker plots with median (horizontal line) and inter-quartile range (boxes) shown. Bars extending to 1.5x the inter-quartile range indicate variance for each parameter while outliers shown as non-connected data points. (B) Dose-response curves depicting variation in dose-response relationships (n=12, Taxol: n=15 for DDM, A2 and B2). Morgan testing indicates a statistically significant difference in the E_{Max} of B2 versus Taxol (F statistic, P= 0.032); although significance diminishes after adjustment for multiple testing.

Fig. 3. Congeners with simplified lactones and monoenes have superior activity relative to DDM in chemorefractory cancer cell models.
(A) Values computed from sigmoidal dose-response curves for 12 cancer cell lines were segregated according to whether cells were dichotomized as Taxol-sensitive (n=9) or -resistant (n=3). Dose response parameters are represented as aligned dot plots indicating median (horizontal line) and inter-quartile range. Bars extending to 1.5x the inter-quartile range are also indicated. Outliers are represented by non-connected data points.

Fig. 4. Superior long-term efficacy of congener B2 in HEY cells

Dose-response curves for DDM, B2 and Taxol in HEY cells after (A) 3 cell doublings (3 days) and (B) 21 days without replenishing compounds or media. Representative images of SRB-stained plates corresponding to 3 days (C) and 21 days (D) are shown. (E) Quantitation of cell-fate in drug-treated HEY cells after 6 days of treatment with DDM, B2 or Taxol. Data were derived by quantifying % of SA-βGal+ cells, a metric of senescence, as a proportion of drug effect. DDM strongly induced senescence relative to Taxol, while B2 induced senescence at an intermediate rate. B2 demonstrated a prolonged anti-cancer effect, evident 3 weeks post dosing.

Fig. 5. Anti-metastatic activity of B2 in chemorefractory TNBC cells.
BT549 cells were exposed to either $EC_{50\ doses}$ (A and B) doses of DDM, B2 or Taxol for 4 days or or E_{Max} doses for 24h (C) and subsequently assayed for metastasis-related endpoints. (A) SRB-stained cells show enlarged, flat cells emerging after DDM treatment, consistent with emergence of a senescent phenotype. In contrast B2 and Taxol-treated cells have reduced numbers of surviving cells that do not have the same morphology. (B) Analysis of a 5-gene metastatic signature following the various treatments indicate a statistically significant decrease in expression relative to the effect of either Taxol or DDM. Statistical significance for B2 and Taxol compared to DDM is indicated. (C) 24h treatment of BT549 with Taxol, DDM, or B2 partially suppresses invasion through matrigel. Statistical significance relative to DDM (unpaired t-test) is indicated. Data represent mean ± SD of 3 independent experiments.

Fig. 6. Structure of the tubulin-B2 Complex infers optimal adaptation in the Taxane-binding pocket.
(A) Close-up view of the interactions observed between congener B2 (yellow) and β-tubulin in white stick and ribbon representation. Hydrogen bonds are depicted as black dashed lines, water molecules as red spheres. (B) Close-up view of the superimposed tubulin–DDM (violet purple) and (C) paclitaxel-stabilized microtubule (pale cyan, PDB ID 5SYF) complexes in stick and ribbon representation. The complexes were superimposed onto their corresponding taxane-site residues 208-219, 225-237, 272-

276, 287-296, 318-320 and 359-376 ($rmsd_{DDM}$ 0.12 [45 C_α-atoms]; $rmsd_{paclitaxel}$ 0.9 [49 C_α-atoms]).

	HEY			A549		
	Fluorescence Intensity (χ)	± SD	*P*	Fluorescence Intensity (χ)	± SD	*P*
DDM	435	163.7	-	415	59.5	-
Taxol	1667	468.3	****	1546	522.8	ns
A1	173	22.0	****	145	11.1	**
A2	177	18.1	***	146	11.0	*
A3	172	44.7	**	148	6.6	*
B1	221	32.0	**	204	39.4	*
B2	199	21.1	***	170	16.2	**
B3	184	33.9	**	161	12.2	*
H_2O_2	1978	257.3	****	1703	116.0	*

Table 1: ROS Generation in DDM- and congener-treated cells.
Ovarian cancer cells (HEY) and NSCLC cells (A549) were treated with E_{Max} doses for 3h, prior to loading with 10μM H2DCFDA to detect intracellular ROS (measured as fluorescence intensity). Taxol induced ROS at levels comparable to H_2O_2, while DDM induced ROS to a lesser extent. All congeners had statistically significantly reduced ROS activation compared to DDM in both cell lines (Dunnett's multiple comparison test). There was no statistically significant difference in ROS between congeners (e.g. A1 versus A2) for either cell line (not shown). Data represent mean ± SD of 3 independent experiments.H_2O_2-treated cells were used as a positive control.

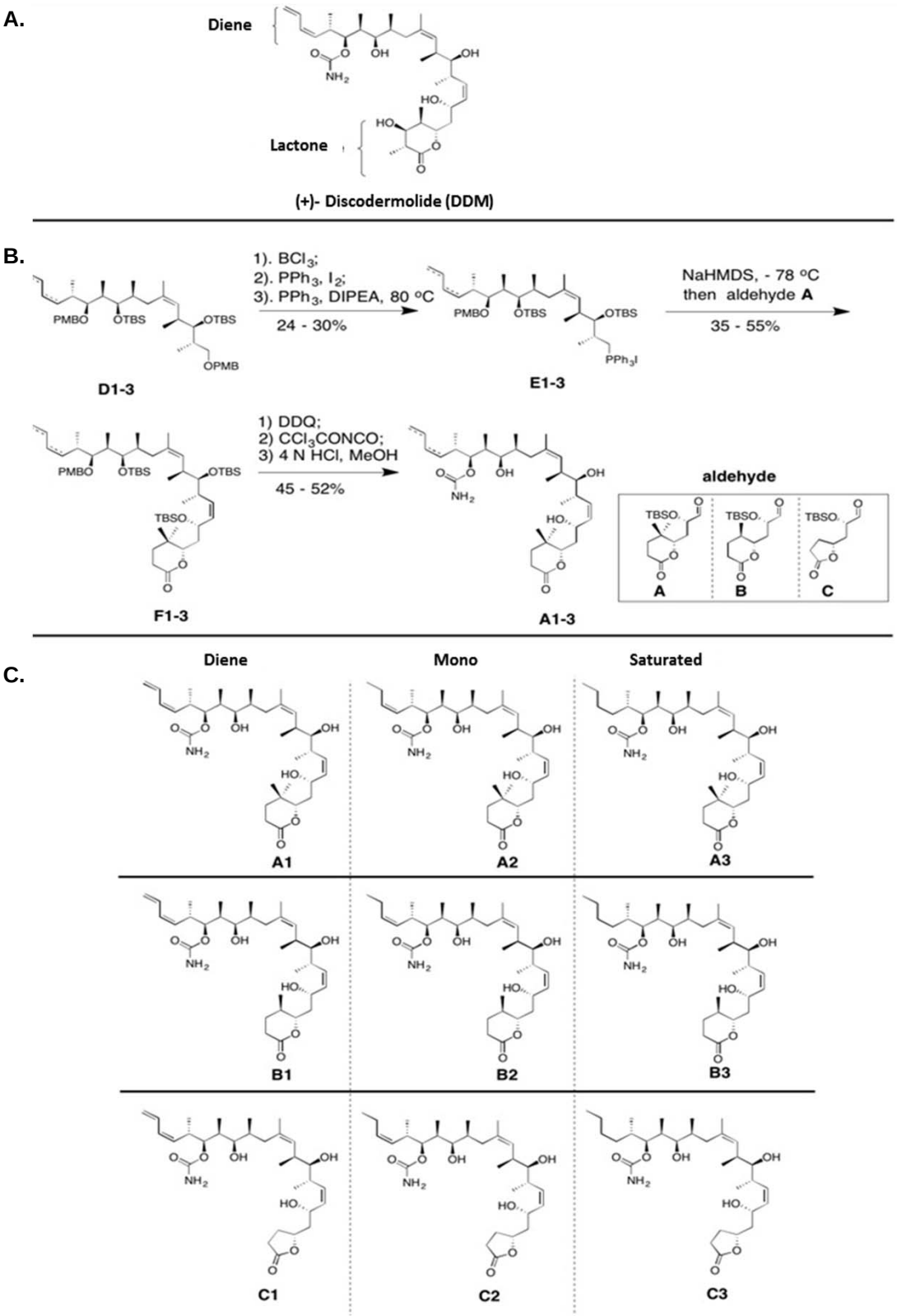
A.
Diene
Lactone
(+)- Discodermolide (DDM)
B.
PMBO
OTBS
OTBS
OPMB
D1-3
1). BCl_3;
2). PPh_3, I_2;
3). PPh_3, DIPEA, 80 °C
24 - 30%
E1-3
NaHMDS, - 78 °C
then aldehyde A
35 - 55%
TBSO
F1-3
1) DDQ;
2) CCl_3CONCO;
3) 4 N HCl, MeOH
45 - 52%
A1-3
aldehyde
A
B
C
C.
Diene
Mono
Saturated
A1
A2
A3
B1
B2
B3
C1
C2
C3

Figure 1

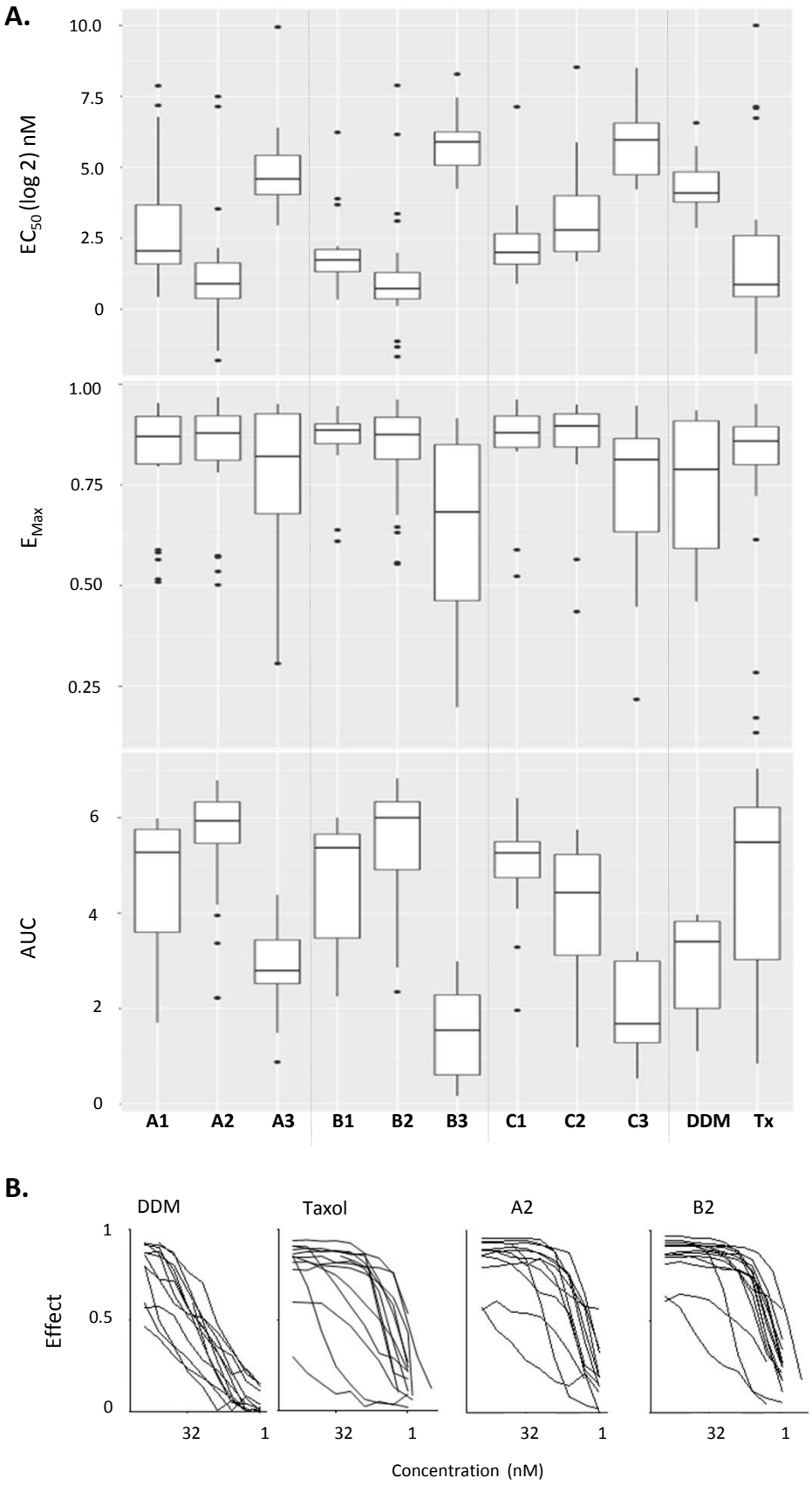
A.
EC50 (log 2) nM
10.0
7.5
5.0
2.5
0
EMax
1.00
0.75
0.50
0.25
AUC
6
4
2
0
A1
A2
A3
B1
B2
B3
C1
C2
C3
DDM
Tx
B.
DDM
Taxol
A2
B2
Effect
1
0.5
0
32
1
Concentration (nM)

Figure 2

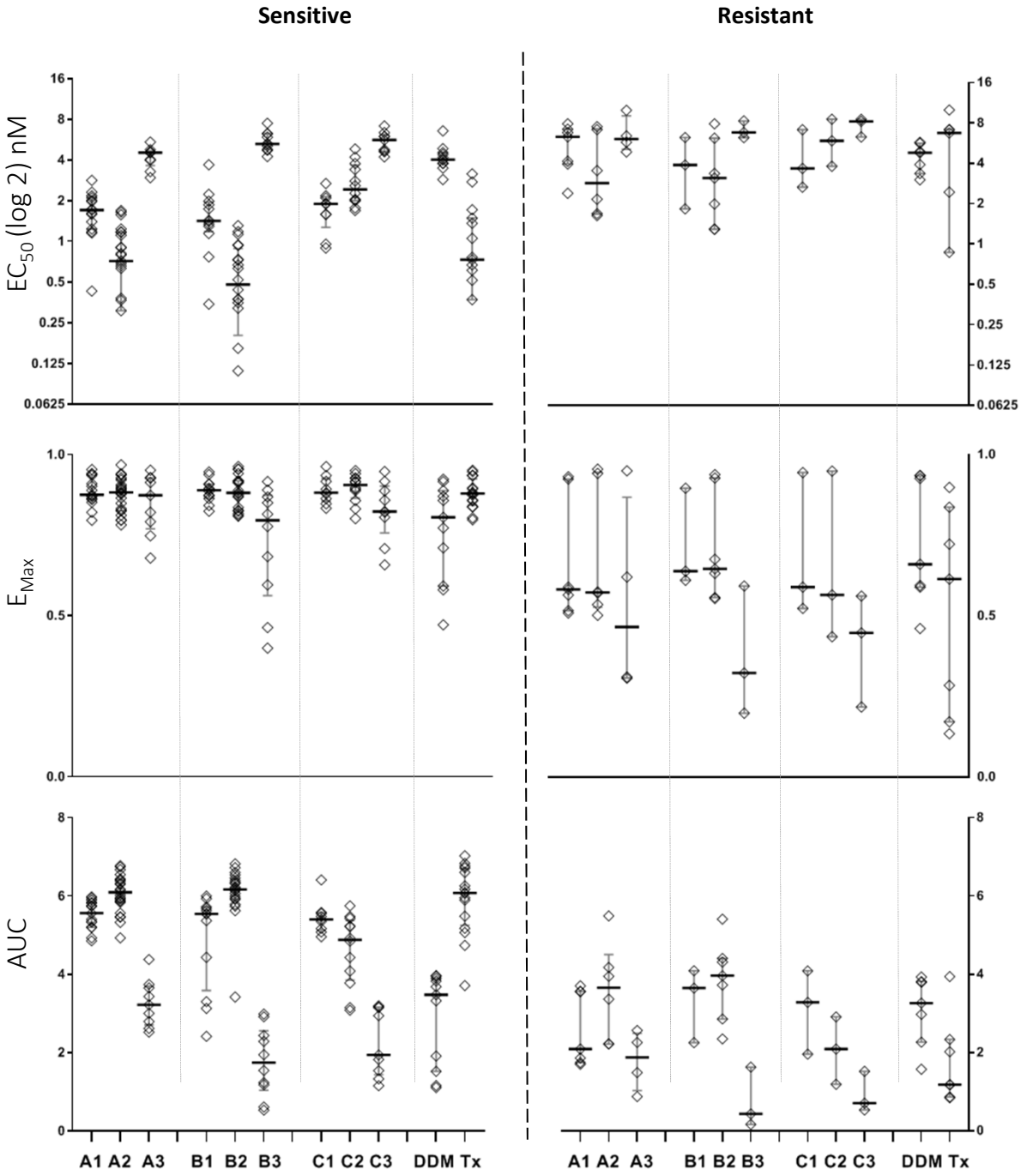
Sensitive
Resistant
EC50 (log 2) nM
EMax
AUC
16
8
4
2
1
0.5
0.25
0.125
0.0625
1.0
0.5
0.0
8
6
4
2
0
A1 A2 A3 B1 B2 B3 C1 C2 C3 DDM Tx

Figure 3

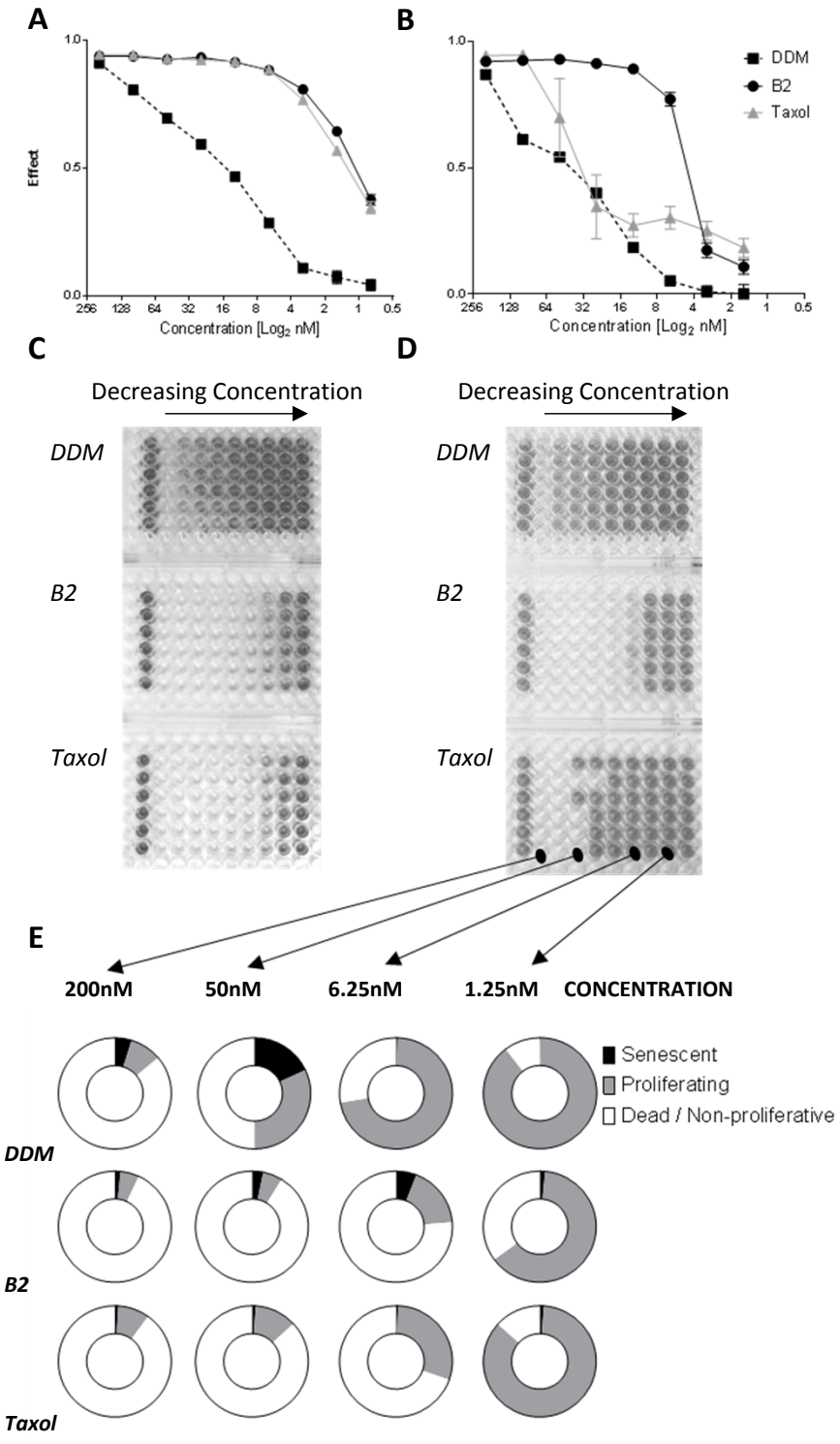
A
B
Effect
Concentration [Log2 nM]
DDM
B2
Taxol
C
D
Decreasing Concentration
Decreasing Concentration
DDM
B2
Taxol
DDM
B2
Taxol
E
200nM
50nM
6.25nM
1.25nM
CONCENTRATION
Senescent
Proliferating
Dead / Non-proliferative
DDM
B2
Taxol

Figure 4

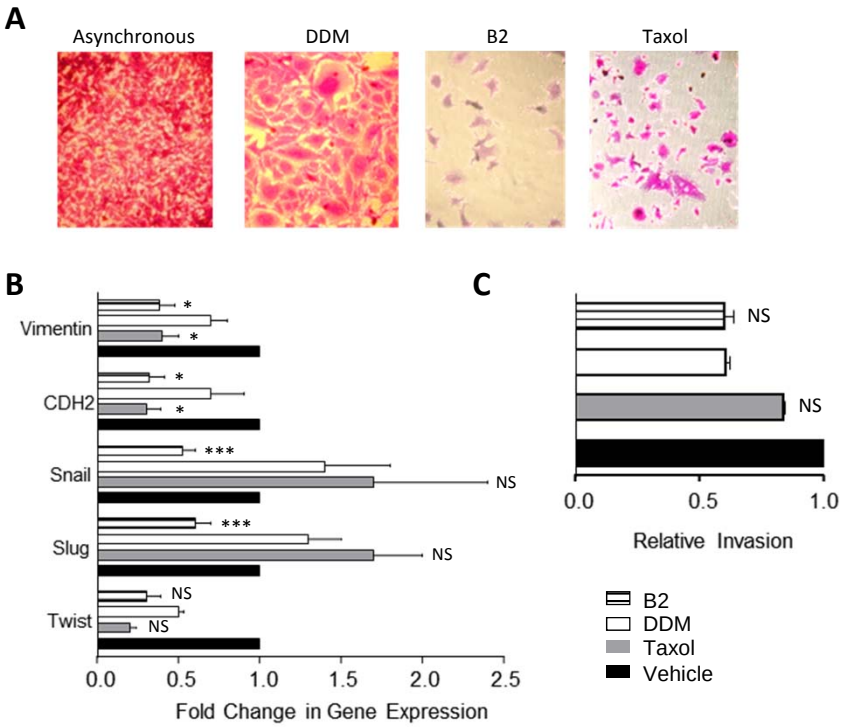
A
Asynchronous
DDM
B2
Taxol
B
Vimentin
CDH2
Snail
Slug
Twist
*
***
NS
0.0
0.5
1.0
1.5
2.0
2.5
Fold Change in Gene Expression
C
NS
0.0
0.5
1.0
Relative Invasion
B2
DDM
Taxol
Vehicle

Figure 5

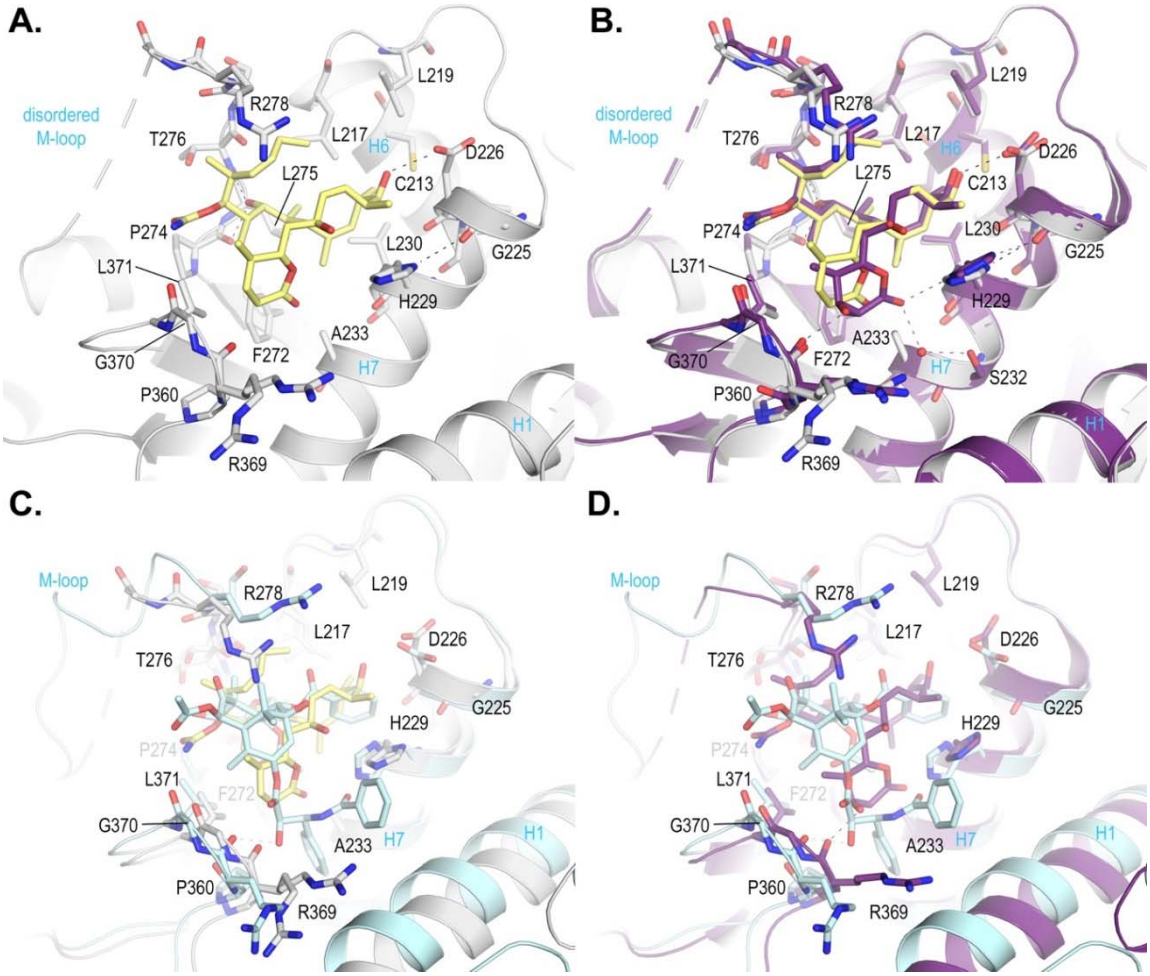
A.
disordered
M-loop
R278
L219
T276
L217
H6
D226
L275
C213
P274
L230
G225
L371
H229
A233
G370
F272
H7
P360
H1
R369
B.
disordered
M-loop
R278
L219
T276
L217
H6
D226
L275
C213
P274
L230
G225
L371
H229
A233
G370
F272
H7
S232
P360
H1
R369
C.
M-loop
R278
L219
L217
D226
T276
G225
H229
P274
L371
F272
G370
A233
H7
H1
P360
R369
D.
M-loop
R278
L219
L217
D226
T276
G225
H229
P274
L371
F272
G370
A233
H7
H1
P360
R369

Figure 6